Published in final edited form as:
Bioconjug Chem. 2008 January ; 19(1): 192–200. doi:10.1021/bc700291m.

The agonist-antagonist dilemma in molecular imaging: Evaluation of a monomolecular multimodal imaging agent for the somatostatin receptor

W. Barry Edwards, **Baogang Xu**, **Walter Akers**, **Phillip P. Cheney**, **Kexian Liang**, **Buck E. Rogers**, **Carolyn J. Anderson**, and **Samuel Achilefu**†
Department of Radiology, Washington University School of Medicine, St. Louis, MO 63110

Abstract

The combination of different imaging modalities, each providing information according to its strengths, can be a powerful method for diagnosing diseases. We have synthesized a monomolecular multimodal imaging agent (MOMIA), LS172, containing a subtype-2 somatostatin receptor (SSTr2)-avid peptide (Y3-octreotate or Y3-TATE), a radiometal chelating group (DOTA) and a near-infrared (NIR) fluorescent dye (cypate). In addition to optical methods, radiolabeling LS172 with ^{64}Cu and ^{177}Lu provides a strategy for in vitro evaluation or in vivo multimodal imaging by positron emission tomography (PET) and single photon emission computed tomography (SPECT), respectively. Determination of the binding affinity of LS172, ^{nat}Cu- and ^{nat}Lu-LS172 in SSTr2-transfected A427 cells (A427-7) showed that they all displayed high binding affinity toward SSTr2 with K_i values of 0.234 nM, 11.5 nM, and 2.15 nM respectively. In contrast to cypate-labeled Y3-TATE (cytate), fluorescence microscopy showed that LS172 and ^{nat}Cu-LS172 accumulate modestly in A427-7 cells by SSTr2-mediated endocytosis, in spite of their relatively high binding affinity. In vivo, the biodistribution of the SSTr2 receptor specific ^{64}Cu- and ^{177}Lu-LS172 in AR42J tumor bearing rats exhibited low (≤1% ID/g) accumulation in tumor tissue. Clearance from circulation was predominantly hepatobiliary (>90% ID/liver). Both optical and radionuclear biodistribution studies showed a similar in vivo distribution profile. Surprisingly, the strong binding of LS172 to SSTr2 did not translate into high SSTr2-mediated endocytosis in cells or uptake in tumor in vivo. Considering that LS172 is a putative antagonist, the poor accumulation of the labeled MOMIAs in SSTr2 positive tumor tissue supports the paradigm that agonists with their concomitant internalization favors appreciable target tissue accumulation of receptor-specific ligands.

INTRODUCTION

Accurate diagnosis and treatment of diseases may be achieved by integrating multimodal imaging strategy as part of the therapeutic regimen. With the aid of fast computational methods and algorithms for image reconstruction, co-registration of diseased tissue images can yield complimentary information, thus enhancing diagnosis. For example, computed tomographic images (CT) can be co-registered with positron emission tomographic images (PET) or single photon emission computed tomography (SPECT) (1,2). In this way, the combination of anatomical information from CT with functional information from PET or SPECT, allows cancers to be staged and precisely localized.

Optical imaging is an emerging method that could act synergistically with another imaging modality. Optical imaging itself is a highly sensitive technique that can detect, in vitro as well

†corresponding author, 4525 Scott Avenue, St. Louis, MO 63110, Phone: 314-362-8599, Fax: 314-747-5191, achilefus@mir.wustl.edu.

as in vivo, minute quantities of light-emitting materials. Additionally, it uses low energy radiation in the visible or near-infrared (NIR) regions of light to assess biological processes. As the light penetrates deeper in tissues, tissue chromophores, cellular organelles, and matrix mediate scattering and absorption of emitted light. While algorithms can deconvolute light propagation through tissues, accurate models of the complex photon migration in heterogeneous biological systems are not available. This limitation would benefit from pairing optical with another imaging modality such as PET. By coupling together an optical and a radionuclear method, the location of a target tissue could first be confirmed by PET then monitored longitudinally by optical imaging for such changes as tumor response to therapy.

Previously, we and others have developed near-infrared fluorescent and radiolabeled monomolecular multimodal imaging agents (MOMIAs) for combined optical-radionuclear small animal imaging (3–5). Typically, these MOMIAs were labeled with gamma-emitting ^{111}In for scintigraphy or SPECT. These studies demonstrated the capability of obtaining co-registered images of the distribution of the MOMIAs in small animals by both fluorescence and gamma imaging methods. However, previous studies focused on using the MOMIA strategy for multimodal imaging. Interestingly, the ability of some radionuclides to emit photons for imaging and therapeutic applications provides a strategy to incorporate therapeutic radionuclides into the MOMIA concept. This can be accomplished by using ^{177}Lu or ^{64}Cu radiometals in MOMIA constructs.

^{177}Lu ($t_{½}$ = 6.65 d) has gamma emissions (208 keV; 11%) for SPECT imaging and therapeutic properties (β-, 497 keV; 78%). A peptide conjugate of this radiometal, ^{177}Lu-DOTA-Y3-TATE, has demonstrated excellent tumor localization and good clearance properties, as well as significant tumor regression in an animal model (6,7). SPECT has many advantages as an imaging method but PET is the current method of choice for both human and small animal molecular imaging because of its exceptionally high sensitivity and in vivo quantitative measurements of the early kinetics of drug distribution. A widely used radiometal for PET is ^{64}Cu because of it's convenient half-life ($t_{½}$ = 12.7 h) and decay properties (β^+ (19%); β^-(39%)) that are suitable for PET as well as radiotherapy. Both radiometals form stable complexes with tetraazamacrocycle DOTA, which can be conjugated to bioactive molecules such as peptides and proteins for specific delivery to target tissue (7–10).

To take advantage of the multimodal approach, we have developed a single imaging agent that contains reporters for both optical and SPECT or PET imaging modalities as well as radiotherapeutic properties. These MOMIAs offer minimization of data analysis errors due to differences in the pharmacokinetics of two different imaging agents used for each modality, sources of error resulting from interaction of the two imaging probes in vivo, and patient toxicity from repeated administration of multiple probes.

Toward this goal, we chose the well characterized somatostatin receptor subtype-2 (SSTr2) as a target and an oactapeptide Y3-TATE as the targeting ligand (11,12). Y3-TATE has been labeled with a variety of radiometals for diagnostic imaging and radio-therapy, utilizing macrocyclic chelators usually conjugated to the *N*-terminal amine (6,7). For optical imaging, we used the near infrared fluorescent dye cypate (13). Cypate, when conjugated to the N-terminus of Y3-TATE (cytate, Figure 1), was shown by optical imaging to localized in subcutaneous SSTr2-positive tumors in rat with high selectivity (14). The NIR spectral properties of cypate match the low absorption of intrinsic naturally occurring molecules, resulting in an overall enhancement of signal.

The three-component molecular design (receptor-avid peptide, radiometal chelate, and NIR fluorescent dye) was synthesized on solid support, where DOTA was conjugated to the *N*-terminal amine of D-Phe and cypate was conjugated to the ε-amino group of a *C*-terminal

lysine. The resultant MOMIA, LS172 (Figure 1), was evaluated for its ability to displace ^{111}In-DTPA-Y3-TATE in an in vitro binding assay. After radiolabeling with either ^{64}Cu- or ^{177}Lu-, LS172 was evaluated in a well characterized tumor model (AR42J) for in vivo tumor localization and clearance properties (9,10,15,16). Finally, the cellular internalization of LS172 and ^{nat}Cu-LS172 was determined by fluorescence microscopy. Together, the results demonstrate that the measured high receptor binding affinity of LS172 did not translate into high cellular internalization or in vivo tumor uptake mediated by somatostatin receptor, suggesting that LS172 is an antagonist.

EXPERIMENTAL PROCEDURES

Materials

Chemicals were obtained from Sigma-Aldrich (St. Louis, MO) unless noted differently. Amino acids were purchased from Novabiochem (San Diego, CA). Cypate and cytate were synthesized as previously described (14,17). ^{64}Cu was produced on a CS-15 biomedical cyclotron at the Washington University School of Medicine. ^{177}Lu was obtained from Missouri Resource Reactor (Colombia, MO). The SSTr2-positive A427-7 cells were supplied by B.E. Rogers (18). ^{125}I-SS-14 (^{125}I-iodotyrosil-11-somatostatin-14) was purchased from GE Healthcare (Piscataway, NJ). Protein assays were performed using the BCA assay (Pierce, Rockford, IL). Peptides were analyzed by reversed phase-HPLC (RP-HPLC) on a system consisting of a binary pumping system (Shimadzu LC-10AD, Solvent A=H_2O, 0.1 %TFA and Solvent B=acetonitrile, 0.1% TFA), UV/Vis (Shimadzu SPD-20AV) and fluorescence (Shimadzu RF-10AXL) detectors, and electrospray ionization mass spectrometer (Shimadzu LCMS-2010A).

Peptide Synthesis

LS172 was synthesized entirely on resin with an ACT APEX 396 peptide synthesizer by standard Fmoc protocols as previously described (14,19). Briefly, starting with Rink Amide resin (30 μmol), the Fmoc-protected *C*-terminal amino acid (lysine; 75 μmol) was activated with a mixture of the coupling reagents HOBt (75 μmol) and HBTU (75μmol) in the presence of DIEA (150 μmol). Deprotection of the Fmoc protecting group was accomplished with 20% piperidine in DMF. The free carboxylic acid of tri-t-butyl-DOTA was coupled to the *N*-terminal amine. The orthogonal 4,4-dimethyl-2,6-dioxocyclohex-1-ylidene (Dde) protecting group, which was used to protect the ε-amino group of the *C*-terminal lysine, was removed selectively with 2% hydrazine in dimethylformamide (DMF) before coupling cypate to the resultant free ε-amino group via a carboxylic acid of cypate. Simultaneous removal of side-chain protecting groups and cleavage of the product from solid support was accomplished with a mixture of 95% TFA and 5% water. After lyophilization, the crude product was obtained as a green powder and purified by semi-preparative HPLC. The purity of LS172 was greater than or equal to 96% after RP-HPLC purification (based on UV peak area 217 and 280 nm), calculated M=2169, observed, $[M]^{2+}$, 1085,$[M]^{3+}$, 724. LS172 was quantified based on the extinction co-efficient of cypate in 20% DMSO (224, 000 $M^{-1}cm^{-1}$) (17).

Preparation of ^{nat}Cu- and ^{nat}Lu-LS172

LS172 (26 μg, 12 nmol, 0.91 μg/μL, 20% DMSO) was added to reaction buffer (278 μL, 100 mM NH4OAc, pH 4.0) containing DMSO (80 μL). $LuCl_3$ (14 nmol, 0.4 mg $LuCl_3$-$6H_2O$/mL, 100 mM HCl) was added to prepare ^{nat}Lu-LS172 (20). ^{nat}Cu-LS172, was prepared similarly with $CuCl_2$ (14 nmol, 0.2 mg $CuCl_2$-$2H_2O$/mL, 100 mM HCl) in a more alkaline reaction buffer (279 μL, 100 mM NH_4OAc, pH 5.5) (21). The reactions were monitored by RP-HPLC (Supelco ABZ plus, C-18, 3 μm, 4.6 × 150 mm, linear gradient of 35–55%B, 20 min). ^{nat}Lu-LS172 was formed in >99% conversion and identified by LCMS, but the formation of ^{nat}Cu-LS172 was incomplete (80% conversion), as determined by UV/Vis (780 nm). Therefore, an

aliquot of the reaction mixture (325 μL) was treated with additional $CuCl_2$ (65 nmol, 56.9 μL, 0.2 mg $CuCl_2$-$2H_2O$/mL, 100 mM HCl) and heated (50 °C, 1 h) but no additional conversion was observed. ^{nat}Cu-LS172 was purified by RP-HPLC (3 × ~4 μg portions, Supelco ABZ plus, C-18, 3 μm, 4.6 × 150 mm, linear gradient of 35–55% B, 20 min). The purity of ^{nat}Cu-LS172 was 95% after HPLC purification (based on UV peak area, 780 nm). ^{nat}Lu-LS172 was used without purification because of the complete conversion of LS172 to the metal complex. ^{nat}Cu-BS29, calculated [M]=2232; observed 744, $[M]^{3+}$, 1115, $[M]^{2+}$; ^{nat}Lu-LS172, calculated [M]=2169, observed 781, $[M]^{3+}$, 1170, $[M]^{2+}$.

Radiochemistry

LS172 was radiolabeled with ^{64}Cu as previously described (21). Radiochemical purity of ^{64}Cu-LS172 was ≥ 95% after heating (95 °C, 60 min) and final specific activities were 153 μCi/ug (332 μCi/nmol). ^{177}Lu (100 μCi) was added to labeling buffer (ammonium acetate, 100 mM, pH 5.5) along with LS172 (8 μg, 3.7 nmol) and DMSO (final concentration of 20% by volume). Purity was determined by radio-RP-HPLC (A = water, 0.1 %TFA; B = acetonitrile 0.1% TFA; Vydac 201HS5415, 4.6 × 150 mm, linear gradient 30% to 70% B in 10 min, 1 mL/min). Radiochemical purity of ^{177}Lu-LS172 was ≥ 99% after heating (80 °C, 80 min) and final specific activity was 12.5 μCi/μg (27 μCi/nmol). For receptor binding assays, DTPA-Y3-TATE was radiolabeled with ^{111}In (100 mM NH4OAc, pH 5.5) at a specific acitivity of 700 μCi/μg. Purity was >99% (10% to 75% B, 10 min, linear gradient). Gentisic acid (2,5-dihydroxy-benzoic acid) was added at a final concentration of 1 mM to prevent radiolysis (22).

Spectral Properties of LS172

Excitation and emission spectra were performed on a Jobin-Yvon Flurolog 3 and absorption measurements were performed in Beckman DU-145. Stock solutions (~1 mM) of indocyanine green (ICG) and LS172 were prepared in DMSO and serial dilutions were made to obtain an absorbance level of ~0.02 (720 nm). The quantum yield of LS172 (Φ_{LS172}) relative to ICG was determined by the equation $\Phi_{LS172} = \Phi_{ICG}(\text{slope}_{LS172}/\text{slope}_{ICG})$, where the slope is determined from a linear regression of integrated fluorescence intensity (735 to 830 nm) versus absorbance (720 nm) of serially diluted LS172 in DMSO (23,24).

Cell Culture

The A427-7 cell line expressing the human SSTr2 receptor was maintained at 37°C in a humidified atmosphere containing 5% CO_2 in Eagle's Minimal Essential Medium (EMEM) containing 4 mmol/L L-glutamine, 0.1 mM NEAA, 1.0 mM sodium pyruvate, 500 μg/mL G418, 100 U/mL penicillin and 10% fetal bovine serum. HEK293 cells were grown in Dulbecco's modified Eagle's medium (DMEM) containing 100 U/mL penicillin, 4 mmol/L L-glutamine and 10% fetal bovine serum at 37°C in humidified atmosphere containing 5% CO_2.

Fluorescence microscopy and internalization assays

A427-7 and HEK293 cells were grown on 8-well chambers and incubated in EMEM and DMEM culture medium (0.2 mL/well) overnight at 37°C in an humidified atmosphere containing 5% CO_2. Cytate, LS172, and ^{nat}Cu-LS172 were incubated with A427-7 cells at 25 nM or 50 nM in the presence or absence of 5 μM Y3-TATE as a competitor. After 0, 15, 30, 60 and 90 min of incubation (37°C), the slides containing the cells were placed on ice to stop the internalization process, washed (3x) with PBS (4°C, 1 mM Ca^{2+}), fixed (4% paraformaldehyde), and air dried. The fixed cells were then imaged with a confocal microscope (Olympus FV1000) equipped with excitation (775nm/50nm) and emission filters (845nm/55nm) for fluorescence detection in the NIR region. To generate values of relative fluorescence

units (rfu) for internalized dye conjugated peptides, a region of interest was generated by drawing a line (that excluded the cell membrane) spanning the cytoplasm and transversing the region of greatest fluorescence intensity (Olympus FV10-ASW 1.4 software). The rfu are reported as an average of intensity of the drawn line. A cell was arbitrarily chosen from each corner as well as the center of the field as representative sample (n=5). Because the background fluorescence was negligible, it was not subtracted from the total fluorescence.

In vitro binding assay

The receptor binding assays were carried out as previously described (14). For the inhibition assays, varying concentrations of the competitor were incubated with ^{111}In-DTPA-Y3-TATE and membranes enriched in SSTr2 receptor (A427-7, 2 h, ambient temperature). Membrane levels were adjusted so that no more than 10% of the added radioactivity was bound (2.5 μg protein/well). To determine B_{max}, increasing concentrations of ^{125}I-SS-14 were incubated with A427-7 membranes from either cultured cells or from xenografted tumors (10 to 20 μg protein/well). Bound radiotracers were separated from unbound by filtration through fiberglass filter pads (Millipore Multiscreen system). After rinsing, radioactivity in the pads was assessed by gamma counting. The data were fit by non-linear regression to the following equation: Y = bottom + (top−bottom)/(1+10exp(X-logIC_{50})), where Y is cpm bound and X is log concentration. K_i values were obtained with the Cheng-Prussof equation. To determine K_D and B_{max} values, data were fit by non-linear regression to total saturation binding with ligand depletion, where X is the amount of ^{125}I-SS-14 (cpm) added and Y is the total amount (cpm) of radiotracer bound. Non-linear regression calculations were determined with GraphPad Prism (version 4.00 for Windows, GraphPad Software, San Diego, CA).

Radiochemical Biodistribution of MOMIAs

AR42J tumors were implanted bilaterally in the legs of male Lewis rats from donor rats (9). After 10–14 days, the tumors had grown to ~ 1.5 to 2.0 g. ^{64}Cu-LS172 was formulated in 20% DMSO in PBS by volume to prevent adherence of the radioligand to the vessel. ^{64}Cu-LS172 (4 μCi/27 ng/12 pmol/rat, n=5) was administered via the tail vein. Y3-TATE (100 μg/95 nmol/rat, n=4) was included as a competitive dose. ^{177}Lu-LS172 (6.2 μCi/500 ng/230 pmol/rat) was formulated in 20% DMSO in PBS by volume with 10 μg/μL gentisic acid to prevent radiolysis. Y3-TATE (100 μg/95 nmol/rat, n=5) was included as a competitive dose.

Optical imaging and biodistribution

Six 4-week-old male NCR nu/nu mice were anesthetized with ketamine (87 mg/kg) and xylazine (13 mg/kg) via intraperitoneal injection. About 5×10^5 A427-7 cells were injected subcutaneously in the right and left flanks of each mouse. Tumors were allowed to grow to 5–10 mm maximum diameter before treatment. For in vivo imaging, mice were anesthetized with ketamine/xylazine cocktail as described above. LS172 (2 nmol in 100 μl 20% DMSO) was injected intravenously via lateral tail vein, alone (n=3) and with a competitive dose of Y3-TATE (100 μg/95 nmol/mouse) (n=2). In vivo imaging of the treated mice was performed with a multimodal planar imaging system (IS4000MM Eastman Kodak Company, New Haven, CT). Broadband illumination from a 150 W halogen lamp was filtered by 755/35 nm optical bandpass filter (Eastman Kodak Company, New Haven, CT) and the emitted light captured via cooled CCD camera after 830 wide-angle longpass filter (e830WA, Eastman Kodak Company, New Haven, CT). Brightfield and NIR fluorescence images were collected at 1, 4, 8 and 24 h post-injection. Regions of interest (ROIs) were drawn within the areas related to the liver, kidneys, tumor and a control region on the opposite flank for comparison of relative in vivo fluorescence distribution at each time point. After 24 h, the mice were euthanized by cervical dislocation under anesthesia. Tissue samples from muscle, liver, kidney, adrenal gland,

pancreas, spleen, brain, skin and tumor were harvested for ex-vivo fluorescence biodistribution imaging using the same settings as above.

Statistical methods

Mean fluorescence intensities for the two experimental and control groups were compared with unpaired t-tests performed using GraphPad Prism version 4.00 for Windows (GraphPad Software, San Diego, CA).

RESULTS

Synthesis and spectral properties

Y3-TATE is widely used to target somatostatin receptors that are up-regulated in cancer and other pathologic conditions (6,10,19,20). This peptide is typically labeled with radiometal chelators or fluorescent probes for imaging applications. To design radionuclear-optical MOMIA, it would be easier to incorporate a lysine residue at the N-terminus of the peptide to provide two amino groups for conjugating DOTA and cypate. However, in a previous study, we showed that this molecular construct can compromise the peptide's binding affinity for SSTr2 (14). In developing macrocyclic scaffold for molecular optical imaging, we found that adding lysine to the C-terminus of Y3-TATE (Y3-K9-TATE) retained the binding affinity of Y3-TATE (17) and provided a second reactive group for coupling cypate at a distal position to DOTA. Thus, LS172 was prepared by conjugating DOTA and cypate at the N- and *C*-terminal positions of Y3-K9-TATE, respectively. To construct the entire molecule on solid support, we had to use the orthogonal Dde protecting group for lysine. This allowed us to complete the peptide synthesis and DOTA coupling before Dde removal and subsequent conjugation of cypate. The procedure is advantageous because cypate, which is unstable under the basic conditions, was added toward the end of MOMIA synthesis. Thus, exposure of cypate to basic condition was minimized and the subsequent cleavage of the product from solid support was carried out under acidic conditions, where the NIR fluorescent dye is very stable. The structures of LS172 and other compounds used in this study are shown in Figure 1.

LS172 exhibited excellent spectral properties, including similar absorption and emission spectra to the precursor dye cypate (Figure 2). Typical of many heptamethine dyes, LS172 has a narrow Stokes shift (23 nm) but the broad excitation and emission bands allow for a wide range of wavelength choices for excitation or fluorescent detection in biological assays or in vivo imaging (25). The relative quantum yield of LS172 ($\Phi_F = 0.12$) was the same as the reported quantum yield of ICG, indicating that conjugation of cypate to the MOMIA did not compromise detection sensitivity. ^{nat}Cu-LS172 was highly fluorescent and maintained the same fluorescent properties of the parent analog LS172 with minimal Cu-mediated quenching. Both natural and radioactive Cu and Lu were incorporated into LS172 with high radiochemical purity and specific activities for the radiometals.

In vitro receptor binding assays

A heterologous receptor binding assay was performed with A427-7 cell membranes, where ^{111}In-DTPA-Y3-TATE was displaced by various competitors (Table 1, Figure 3A). Utilizing a value of $K_D = 0.13$ nM and a concentration of 0.39 nM, the Cheng-Prussof equation was used to calculate the K_i values for all of the competitors. Cytate, SS-14 and Y3-TATE display affinity for SStr2 in the sub-nanomolar region. The K_i values indicate that LS172 has strong affinity for SSTr2 ($K_i = 2.03$ nM) and the complexation with lutetium had very little effect on the affinity ($K_i = 2.15$ nM). However, addition of copper to the chelator decreased affinity by approximately 5-fold ($K_i = 11.5$ nM).

^{125}I-SS-14 was used to assess the receptor densities of SSTr2 on xenografted and cultured A427-7 cells (Figure 3B). The xenografted cells expressed 2.3 pmol/mg (0.5 to 4.0 pmol/mg 95%CI) while the cultured cells expressed 1.0 pmol/mg (0.3 to 1.7 pmol/mg 95% CI). The K_D of ^{125}I-SS-14 was essentially the same ($p < 0.05$, F-test) for both membrane preparations (0.3 nM, 0.03 to 0.5 nM, 95% CI, cultured A427-7 cells). The non-specific binding was ~2%.

Internalization by fluorescence microscopy

The internalization of the MOMIAs LS172 and ^{nat}Cu-LS172 was evaluated by fluorescence microscopy in the near-infrared region in A427-7 and negative control HEK293 (SSTr2 negative) cells and compared with cytate. Cytate was strongly internalized in a time-dependent manner (Figure 4 and Figure 5) and the internalization was successfully blocked with a competitive dose of Y3-TATE. In contrast, LS172 was weakly internalized at 25 nM. A competing dose of Y3-TATE inhibited its accumulation until later time points (Figure 5). Surprisingly, the ^{nat}Cu-LS172 was not internalized to any significant extent in the cells (Figure 5). The apparent externalization of some of the ligands at the 30 min could be attributed to an error arising from the inherently low fluorescence intensities at this early time point.

Radiochemical Biodistribution

Both ^{64}Cu- and ^{177}Lu-LS172 displayed relatively similar pharmacokinetic profiles with a rapid blood clearance of 0.151 ± 0.027 and 0.228 ± 0.047 %ID/g, respectively, at 1 h post injection (Table 2). Clearance was predominately hepatic for both ^{64}Cu-LS172 (16.824 ± 1.520 %ID/g, 95.8 ± 7.12% ID/liver, 1h) and ^{177}Lu-LS172 (17.862 ± 3.286 %ID/g, 89.6 ± 3.16% ID/live, 1 h) with relatively low kidney accumulation (~1 to 2% ID/g). Accumulation of activity for both radiolabeled MOMIAs in the SSTr2-positive tissues of adrenal, pituitary, pancreas, and tumor (average of left and right) were relatively low (≤1% ID/g) in all cases. ^{64}Cu-LS172 accumulation in tumor decreased with a co-administration of a competitive dose of Y3-TATE in the tumor ($P < 0.05$) but the observed decrease in other SSTr2-positive organs was not significant. The decreases in the accumulation of ^{177}Lu-LS172 in SSTr2-positive tissues with a co-administration of a competitive dose of Y3-TATE were significant ($P < 0.05$) in all target tissues except the bone.

Optical Imaging

The receptor binding assay suggests that Cu chelation reduces the affinity of LS172. Because cypate in this MOMIA provides the NIR fluorescence signal, we were able to assess its relative biodistribution in vivo and ex vivo without metal chelation to delineate the effect of radiolabeling on LS172. Thus, we evaluated the biodistribution of LS172 in A427-7 tumor-bearing mice at 1, 4, 8 and 24 h noninvasively. LS172 rapidly accumulated in the liver and kidneys, with low concentrations detected in the tumor and muscle tissues (Figure 6–Figure 8). At 24 h, representative tissues and organs were harvested and imaged ex-vivo to determine the relative tissue uptake of LS172 (Figure 9). In addition to the liver and kidneys, LS172 accumulated in the spleen and accounted for 35% of the fluorescence intensity relative to the liver (Figure 9). LS172 accumulation in mouse kidney was somewhat higher than that of the radiolabeled analogs in rat kidney, possibly indicating the reduction of overall charge on the DOTA upon chelation with a metal.

In spite of the high SSTr2, in vivo imaging did not show significant tumor accumulation of LS172 relative to normal tissue at different time points (Figure 7) and competitive inhibition with Y3-TATE did not significantly alter the tumor-to-muscle uptake ratio (Figure 8). The uptake and blood clearance profiles of LS172 in tumor bearing A427-7 mice were similar to that of ^{177}Lu-LS172 and ^{64}Cu-LS172 in tumor bearing AR42J tumors. Inhibition studies with a competitive dose of Y3-octreotate showed that the observed uptake of LS172 in all tissues

examined is attributable to nonspecific accumulation, including SSTr2-positive adrenal, pancreas, and tumor tissues (Figure 9).

DISCUSSION

Somatostatin peptide analogs are well characterized as radio-imaging and therapeutic agents for the somatostatin receptor (6,7,10,15). Previous studies have shown that labeling these peptides with fluorescent dyes provides a method to image SSTr2-positive tumors in mice (14,19,26). The goal of this work was to determine whether a somatostatin peptide analog, labeled with a radiometal and a NIR fluorescent dye, would localize in a receptor-specific manner to a target tissue, such as a xenografted tumor. The somatostatin analog was chosen based on the structure of Y3-TATE, where the tetraazamacrocycle, DOTA, was conjugated to the *N*-terminal D-phenylalanine residue and the near infrared dye, cypate, was conjugated to the ε-amino group of lysine at the C-terminus. This compound, LS172, was used for NIR fluorescence imaging or labeled with ^{64}Cu and ^{177}Lu and evaluated in tumor bearing rats by nuclear methods. In addition, LS172 was also metallated with the natural Cu and Lu for receptor binding studies as well as cell uptake experiments.

In the receptor binding studies, ^{nat}Cu-LS172 and ^{nat}Lu-LS172 were used to displace ^{111}In-DTPA-Y3-TATE (Table 1, Figure 3A). The IC_{50} values were converted to K_i values and compared to those of Y3-TATE, cytate and SS14. The addition of cypate to the *N*-terminus of Y3-TATE (cytate) did not significantly change the binding affinity. However, modifications of both the N- and C-termini decreased the binding affinity of LS172 by about 10- and 5-fold relative to cytate and Y3-TATE, respectively. Moreover, while the complexation of ^{nat}Lu with DOTA had little effect on affinity, complexation of ^{nat}Cu reduced the affinity of LS172 by approximately 5-fold. In spite of the fact that the SSTr2-binding amino acid sequence of the peptide, the Phe (or Tyr)- D-Trp-Lys-, is relatively isolated from the termini, modifications at these sites still can affect binding. Previous studies have shown that the addition of the peptide PKKKRKV(OH) via an aminohexanoic acid linker to the *C*-terminal threonine residue of DOTA-Y3-TATE resulted in a relatively weak binding peptide when labeled with ^{111}In (K_D ~280 nM) (27). Furthermore, DOTA-Y3-octreotide was a weaker competitor (IC_{50}= 14 ± 2.6, SEM) toward radio-iodinated SS-14 than DOTA-Y3-TATE (IC_{50}= 1.5 ± 0.4 nM, SEM), indicating that the relatively small change from the *C*-terminal alcohol to that of the carboxylic acid can result in a nearly 10-fold increase in affinity (28). Changing the radiometal in the chelator can also affect affinity. ^{nat}Ga-DOTA-Y3-octreotide bound the SSTr2 subtype with 5-fold higher affinity than the corresponding Y^{3+} derivative. This difference was ultimately attributed to a conformational change in the *N*-terminal D -Phe residue of the Y^{3+} analog as a result of binding of the amide D-Phe carbonyl oxygen in the metal coordination sphere (29). Nevertheless, the observed affinities of ^{nat}Cu-LS172 and ^{nat}Lu-LS172 are sufficiently strong for receptor imaging and therefore they were radiolabeled with the corresponding radioisotopes and investigated in animal cancer models.

A well characterized tumor model, AR42J rat pancreatic xenografts, was chosen for evaluating the radiolabeled MOMIA. This model has been successful and reliable in the evaluation of a variety of radiolabeled somatostatin analogs targeted to the SSTr2 with the added benefit of confirming receptor specific uptake in SSTr2 rich organs of adrenal, pituitary and pancreas (9,10,15,16). Previous investigations of radiolabeled somatostatin analogs showed uptakes in AR42J xenografts that ranged from low ~1% ID/g up to ~6% ID/g. For example, the accumulation of ^{64}Cu-DOTA-D-Y1-octreotate (K_D = 0.2 nM) at 1 h was 1.52% ID/g and decreased to 0.468% ID/g with a competing dose of D-Y1-TATE (9). On the other hand, SSTr2-positive tissue uptake in pituitary, adrenal, and pancreas was 1.99, 1.37, and 1.49% ID/g respectively with concomitant decreases upon co-administration of a competing dose of unlabeled Y1-TATE. In another study, ^{64}Cu-TETA-Y3-TATE accumulation in AR42J

xenografts at 1 h was ~1.7% ID/g with observed accumulation in pancreas and adrenals ~3.0 and 2.5% ID/g, respectively. A competing dose of Y3-TATE resulted in >90% inhibition of accumulation in these tissues (16). The observed accumulation of ^{64}Cu-LS172 in AR42J xenografts was lower, uniformly less than 1% (Table 2). Furthermore, while co-administration of a competing dose of Y3-TATE resulted in decreased uptake in all SSTr2-positive tissues, the results were significant only for the xenografted AR42J tumors ($P < 0.05$, two-tailed unpaired t-test). Other features of the ^{64}Cu-LS172 biodistribution included relatively rapid blood clearance (1 h), predominantly hepatobiliary clearance, and relatively high spleen uptake.

The biodistribution of ^{177}Lu-LS172 bore many similarities with that of ^{64}Cu-LS172, including clearance pathways and rates, high spleen uptake, and lower SSTr2-positive tissue uptake (≤ 1%; Table 2). The exception was that SSTr2-positive tissue uptake of ^{177}Lu, except for bone, was inhibited by a competitive competing dose of Y3-TATE ($P < 0.05$, two-tailed un-paired t-test). For comparison, the accumulation of ^{177}Lu-DOTA-Y3-TATE in pancreas, adrenals, and bone (femur) at 1 and 4 h was ≥ 10% (6,7). Competing doses of octreotide at later time points confirmed that the accumulation was receptor specific (6). Specific activity is not considered a likely confounding factor in this study because the specific activity was 3.5-fold less (27 μCi/nmol) than the reported specific activity (94 μCi/nmol) where high accumulation in bone and pancreas were observed (7). While saturation assays on dissected AR42J xenografts were not performed to verify that they retained expression of SSTr2, the low accumulation of both ^{64}Cu- and ^{177}Lu-LS172 in other SSTr2-positive tissues demonstrates the poor specific uptake of LS172 in vivo. For these reasons, biodistribution of the radiolabeled LS172 at later time points were not performed in this study.

Surprised by the in vivo outcome using AR42J cells, we explored the use of an alternative cell line rich in SSTr2. We recently developed a new cell line, A427-7 (A427 clone 7) that meets our need (18). SSTr2 was transfected into A427 cells with relatively large receptor numbers (~7.0 pmol/mg protein). The transfected receptor appeared to function identically to the wild type receptor because recent studies with SSTr2-avid ^{64}Cu-TETA-octreotide showed it was internalized by A427-7 cells and had relatively high SSTr2 specific accumulation in vivo (18). Therefore, this cell line provides a method to evaluate the MOMIAs in another cell line.

Considering that the SSTr2 binding assay demonstrated that radiolabeling of LS172 with Cu reduced the affinity, we imaged the distribution and uptake of the NIR fluorescent LS172 in A427-7 tumor bearing nude mice by fluorescence imaging. The LS172 was administered to the mice with and without a competing dose of Y3-TATE. This allowed us to determine whether the radiometal played a role in the relatively low tumor accumulations in AR 42J cells in rat.

Longitudinal, non-invasive optical imaging provided relative biodistribution data at multiple times during the 24 h after injection (Figure 7). Despite these changes, in vivo optical imaging showed that LS172 accumulation paralleled that of the radiochemical biodistribution with relatively rapid blood clearance and predominant hepatobiliary clearance with no apparent receptor specific accumulation in A427-7 tumor or other SSTr2-positive tissues. In vivo and ex vivo fluorescence imaging did not show significantly higher LS172 accumulation in tumor tissue relative to healthy tissues (Figure 6–Figure 9). The observed increase in kidney retention relative to the radionuclear biodistribution could be attributed to species differences. Alternatively, the absence of metals in LS172 increases the net negative charge on DOTA, thereby favoring kidney uptake.

To determine whether the low accumulation of LS172 in the A427-7 cells was due to receptor down-regulation, saturation assays with ^{125}I-SS-14was performed on homogenized A427-7

tumors dissected from mice. The results showed robust expression of SSTr2 (2.3 pmol/mg), indicating that receptor loss in the xenografts was not the cause of the low observed tumor accumulation (Figure 3B). Our observed values of SSTr2 receptor densities in the xenografted tumors were lower than the reported values (18). The difference could be attributed to differences in the method used for these measurements. Whereas we determined receptor expression level with ^{125}I-SS-14, the reported values were determined with ^{64}Cu-TETA-octreotide.

Recently, saturation assays with radiolabeled SSTr2 agonists and antagonists identified differing receptor densities, raising the intriguing possibility that there are differing active receptor conformations that are dependent on the radioligand (27). These observations may further explain the differing levels of receptor identified in this work relative to that previously determined (18).

Because it was unusual that ligands with such high affinity failed to localize to receptor rich tissues in vivo, we investigated the uptake of LS172 and ^{nat}Cu-LS172 relative to cytate in A427-7 cells in vitro. Cytate was included as a reference because of its high SSTr2 specific accumulation in a xenografted tumor (CA20948) tumor in as little as 90 minutes (14,19). The internalization of LS172 and ^{nat}Cu-LS172 by A427-7 cells was directly observed by NIR fluorescence microscopy because they are both conjugated to cypate (Figure 4 and Figure 5). Expectedly, cytate was rapidly internalized in A427-7 cells. While LS172 also internalized, it did so at a far slower rate and to a much lower extent than cytate. Internalization of cytate and LS172 was inhibited with a competitive dose of Y3-TATE, thus demonstrating the endocytosis was mediated by the SSTr2 receptor. Lack of observed internalization of either cytate or LS172 in the SSTr2-negative HEK293 cells further confirmed the involvement of SSTr2-specific uptake in A427-7 cells. However, it should be noted that HEK293 cells express low levels of SSTr2 (30).

The hallmark of agonism is the internalization of the receptor-ligand complex (12,15). Antagonists do not stimulate internalization. LS172, with its extremely weak internalization properties, and Cu-LS172 appear to be antagonists and cytate an agonist. Recently, the correlation between agonism, defined as the ability of a putative agonist to inhibit forskolin stimulated cAMP production, and internalization was investigated (31). The concentration required to stimulate internalization was determined by ELISA. Both methods linked these abilities to the concentration required to obtain 50% effect (EC_{50}). The EC_{50} ratio of internalization to cAMP inhibition of SS-28 and SS-14 were ~1. However, for other ligands, such as octreotide, the ratio rose to ~10 indicating that octreotide is 10-fold better at stimulating adenylate cyclase than stimulating receptor internalization. These results show that inhibition of cAMP production may not be the best approach to determine the ability of an agonist to stimulate receptor internalization.

Internalization is considered a key feature for successful in vivo accumulation of the radiotracer at the target site (15). The rationale is that after binding of the radiotracer, the receptor-ligand complex internalizes into an endocytotic pathway while the unbound ligand clears from blood and nontarget tissues. Recently, a high degree of correlation between the rate of internalization of SSTr2-avid ligands in vitro and accumulation in SSTr2 enriched xenograft (AR42J) and natural organ (pancreas) in vivo was observed (10). Moreover, successful imaging and therapy with radiolabeled somatostatin analogs in humans have utilized tracers that were internalized in vitro (32,33). Therefore, the low accumulation of LS172 and ^{64}Cu-LS172 in xenografted tumors in vivo appeared to be due to a lack of internalization of these apparent antagonists, while the high receptor specific accumulation of cytate is due to its ability to internalize.

This result stands in sharp contrast to a recent observation that an antagonist (^{111}In-DOTA-SSTr2-ANT) accumulated to a high level (~29 % ID/g, 4 h) in SSTr2 positive tumor xenografts (HEK-SSTr2 transfected tumors in nude mice) (34). The accumulation exceeded that of ^{111}In-DOTA-Y3-TATE (~16 % ID/g, 4h). The authors determined that ^{nat}In-DOTA-SSTr2-ANT was an antagonist by its inability to inhibit forskolin stimulated cAMP production as well as by its inability to stimulate SSTr2 internalization (immuno-fluorescence microscopy). Part of the explanation was that the higher number of receptors identified by the antagonist (15-fold more than the agonist) offset the internalization effect. Unfortunately, the receptor concentrations were not normalized to protein weight, which makes a comparison with our current results difficult. The A427-7 cell line maintained robust expression of the SSTr2 as a xenograft and this high expression level (2.3 pmol/mg) did not offset the lack of internalization of LS172.

In conclusion, LS172, a monomolecular multimodal imaging agent, was radiolabeled with both ^{64}Cu and ^{177}Lu and evaluated as an SSTr2 receptor imaging agent by both optical and radionuclear methods in vitro and in vivo. All the compounds have high SSTr2 binding affinity and retained their fluorescence properties before and after labeling with metal. In spite of the high expression level of the target, LS172 along with its radiolabeled analogs, ^{64}Cu- and ^{177}Lu-LS172, did not accumulate in levels commensurate with their high affinity and high target expression in tumor xenografts. Moreover, accumulation in tissues endogenously expressing SSTr2 was also very low. We attribute the low accumulation to lack of internalization of the labeled ligands in a receptor-ligand complex characteristic of successful SSTr2 imaging agents. Although the anticipated receptor mediated accumulation in target tissues was not observed, the excellent agreement between the optical and radiochemical biodistributions demonstrates the utility of multi-modal monomolecular imaging agents (MOMIAs). In addition, the quantitative radionuclear method is useful for validating data from the high throughput qualitative planar optical imaging method. Overall, high receptor binding affinity in vitro is a necessary but not a sufficient criterion for selecting ligands for in vivo imaging application. The use of dual radio-imaging and therapeutic radiometals provides a strategy for monitoring treatment response, initially by either PET or SPECT, followed by optical imaging at later time points.

Supplementary Material

Refer to Web version on PubMed Central for supplementary material.

ACKNOWLEDGEMENT

We thank Dr. Yunpeng Ye for preparing cypate and Mr. Christopher Sherman for the performing the radio-biodistribution study. This study was support in part by the NIH (R33 CA100972, R01 EB1430, R21 CA123537and R01 CA64475).

LITERATURE CITED

1. Gayed IW, Kim EE, Broussard WF, Evans D, Lee J, Broemeling LD, Ochoa BB, Moxley DM, Erwin WD, Podoloff DA. The value of 99mTc-sestamibi SPECT/CT over conventional SPECT in the evaluation of parathyroid adenomas or hyperplasia. J. Nucl. Med 2005;46:248–252. [PubMed: 15695783]
2. Jaffer FA, Weissleder R. Molecular imaging in the clinical arena. J. Am. Med. Assoc 2005;293:855–862.
3. Zhang Z, Achilefu S. Spectral properties of pro-multimodal imaging agents derived from a NIR dye and a metal chelator. Photochem. Photobiol 2005;81:1499–1504. [PubMed: 16120005]
4. Zhang Z, Liang K, Bloch S, Berezin M, Achilefu S. Monomolecular multimodal fluorescence-radioisotope imaging agents. Bioconjug. Chem 2005;16:1232–1239. [PubMed: 16173803]

5. Houston JP, Ke S, Wang W, Li C, Sevick-Muraca EM. Quality analysis of in vivo near-infrared fluorescence and conventional gamma images acquired using a dual-labeled tumor-targeting probe. J. Biomed. Opt 2005;10:054010. [PubMed: 16292970]
6. de Jong M, Breeman WA, Bernard BF, Bakker WH, Schaar M, van Gameren A, Bugaj JE, Erion J, Schmidt M, Srinivasan A, Krenning EP. [177Lu-DOTA(0),Tyr3] octreotate for somatostatin receptor-targeted radionuclide therapy. Int. J. Cancer 2001;92:628–633. [PubMed: 11340564]
7. Lewis JS, Wang M, Laforest R, Wang F, Erion JL, Bugaj JE, Srinivasan A, Anderson CJ. Toxicity and dosimetry of (177)Lu-DOTA-Y3-octreotate in a rat model. Int. J. Cancer 2001;94:873–877. [PubMed: 11745491]
8. Breeman WA, de Jong M, de Blois E, Bernard BF, Konijnenberg M, Krenning EP. Radiolabelling DOTA-peptides with 68Ga. Eur. J. Nucl. Med. Mol. Imaging 2005;32:478–485. [PubMed: 15655678]
9. Li WP, Lewis JS, Kim J, Bugaj JE, Johnson MA, Erion JL, Anderson CJ. DOTA-D-Tyr(1)-octreotate: a somatostatin analogue for labeling with metal and halogen radionuclides for cancer imaging and therapy. Bioconjug. Chem 2002;13:721–728. [PubMed: 12121126]
10. Storch D, Behe M, Walter MA, Chen J, Powell P, Mikolajczak R, Macke HR. Evaluation of [99mTc/EDDA/HYNIC0]octreotide derivatives compared with [111In-DOTA0,Tyr3, Thr8]octreotide and [111In-DTPA0]octreotide: does tumor or pancreas uptake correlate with the rate of internalization? J. Nucl. Med 2005;46:1561–1569. [PubMed: 16157541]
11. Forrer F, Waldherr C, Maecke HR, Mueller-Brand J. Targeted radionuclide therapy with 90Y-DOTATOC in patients with neuroendocrine tumors. Anticancer Res 2006;26:703–707. [PubMed: 16739341]
12. Hofland LJ, Lamberts SW. The pathophysiological consequences of somatostatin receptor internalization and resistance. Endocr. Rev 2003;24:28–47. [PubMed: 12588807]
13. Bugaj JE, Achilefu S, Dorshow RB, Rajagopalan R. Novel fluorescent contrast agents for optical imaging of in vivo tumors based on a receptor-targeted dye-peptide conjugate platform. J. Biomed. Opt 2001;6:122–133. [PubMed: 11375721]
14. Achilefu S, Jimenez HN, Dorshow RB, Bugaj JE, Webb EG, Wilhelm RR, Rajagopalan R, Johler J, Erion JL. Synthesis, in vitro receptor binding, and in vivo evaluation of fluorescein and carbocyanine peptide-based optical contrast agents. J. Med. Chem 2002;45:2003–2015. [PubMed: 11985468]
15. Hofland LJ, Lamberts SW, van Hagen PM, Reubi JC, Schaeffer J, Waaijers M, van Koetsveld PM, Srinivasan A, Krenning EP, Breeman WA. Crucial role for somatostatin receptor subtype 2 in determining the uptake of [111In-DTPA-D-Phe1]octreotide in somatostatin receptor-positive organs. J. Nucl. Med 2003;44:1315–1321. [PubMed: 12902423]
16. Sprague JE, Peng Y, Sun X, Weisman GR, Wong EH, Achilefu S, Anderson CJ. Preparation and biological evaluation of copper-64-labeled tyr3-octreotate using a cross-bridged macrocyclic chelator. Clin. Cancer. Res 2004;10:8674–8682. [PubMed: 15623652]
17. Ye Y, Li WP, Anderson CJ, Kao J, Nikiforovich GV, Achilefu S. Synthesis and characterization of a macrocyclic near-infrared optical scaffold. J. Am. Chem. Soc 2003;125:7766–7767. [PubMed: 12822971]
18. Parry JJ, Eiblmaier M, Andrews R, Meyer LA, Higashikubo R, Anderson CJ, Rogers BE. Characterization of somatostatin receptor subtype 2 expression in stably transfected a-427 human cancer cells. Mol. Imaging 2007;6:56–67. [PubMed: 17311765]
19. Achilefu S, Dorshow RB, Bugaj JE, Rajagopalan R. Novel receptor-targeted fluorescent contrast agents for in vivo tumor imaging. Invest. Radiol 2000;35:479–485. [PubMed: 10946975]
20. Breeman WA, De Jong M, Visser TJ, Erion JL, Krenning EP. Optimising conditions for radiolabelling of DOTA-peptides with 90Y, 111In and 177Lu at high specific activities. Eur. J. Nucl. Med. Mol. Imaging 2003;30:917–920. [PubMed: 12677301]
21. Rogers BE, Bigott HM, McCarthy DW, Della Manna D, Kim J, Sharp TL, Welch MJ. MicroPET imaging of a gastrin-releasing peptide receptor-positive tumor in a mouse model of human prostate cancer using a 64Cu-labeled bombesin analogue. Bioconjug. Chem 2003;14:756–763. [PubMed: 12862428]
22. Edwards WB, Liang K, Xu B, Anderson CJ, Achilefu S. Synthesis and radiolabeling of a somatostatin analog for multimodal imaging. Proc. SPIE 2006;6097:609703, 609701–609708.

23. Demas JN, Crosby GA. Measurement of photoluminescence quantum yields. J. Phys. Chem 1971;75:991–1023.
24. Philip R, Penzkofer A, Baumler W, Szeimies RM, Abels C. Absortion and fluorescence spectroscopic investigation of indocyanine green. J. Photochem. Photobio. A:Chem 1996;96:137–148.
25. Ye Y, Bloch S, Kao J, Achilefu S. Multivalent carbocyanine molecular probes: synthesis and applications. Bioconjug. Chem 2005;16:51–61. [PubMed: 15656575]
26. Becker A, Hessenius C, Licha K, Ebert B, Sukowski U, Semmler W, Wiedenmann B, Grotzinger C. Receptor-targeted optical imaging of tumors with near-infrared fluorescent ligands. Nat. Biotechnol 2001;19:327–331. [PubMed: 11283589]
27. Cescato R, Schulz S, Waser B, Eltschinger V, Rivier JE, Wester HJ, Culler M, Ginj M, Liu Q, Schonbrunn A, Reubi JC. Internalization of sst2, sst3, and sst5 receptors: effects of somatostatin agonists and antagonists. J. Nucl. Med 2006;47:502–511. [PubMed: 16513620]
28. Reubi JC, Schar JC, Waser B, Wenger S, Heppeler A, Schmitt JS, Macke HR. Affinity profiles for human somatostatin receptor subtypes SST1-SST5 of somatostatin radiotracers selected for scintigraphic and radiotherapeutic use. Eur. J. Nucl. Med 2000;27:273–282. [PubMed: 10774879]
29. Deshmukh MV, Voll G, Kuhlewein A, Macke H, Schmitt J, Kessler H, Gemmecker G. NMR studies reveal structural differences between the gallium and yttrium complexes of DOTA-D-Phe1-Tyr3-octreotide. J. Med. Chem 2005;48:1506–1514. [PubMed: 15743193]
30. Law SF, Yasuda K, Bell GI, Reisine T. Gi alpha 3 and G(o) alpha selectively associate with the cloned somatostatin receptor subtype SSTR2. J. Biol. Chem 1993;268:10721–10727. [PubMed: 8098703]
31. Liu Q, Cescato R, Dewi DA, Rivier J, Reubi JC, Schonbrunn A. Receptor signaling and endocytosis are differentially regulated by somatostatin analogs. Mol. Pharmacol 2005;68:90–101. [PubMed: 15855408]
32. Beutler D, Avoledo P, Reubi JC, Macke HR, Muller-Brand J, Merlo A, Kuhne T. Three-year recurrence-free survival in a patient with recurrent medulloblastoma after resection, high-dose chemotherapy, and intrathecal Yttrium-90-labeled DOTA0-D-Phe1-Tyr3-octreotide radiopeptide brachytherapy. Cancer 2005;103:869–873. [PubMed: 15641034]
33. Bodei L, Paganelli G, Mariani G. Receptor radionuclide therapy of tumors: a road from basic research to clinical applications. J. Nucl. Med 2006;47:375–377. [PubMed: 16513604]
34. Ginj M, Zhang H, Waser B, Cescato R, Wild D, Wang X, Erchegyi J, Rivier J, Macke HR, Reubi JC. Radiolabeled somatostatin receptor antagonists are preferable to agonists for in vivo peptide receptor targeting of tumors. Proc. Natl. Acad. Sci. U. S. A 2006;103:16436–16441. [PubMed: 17056720]

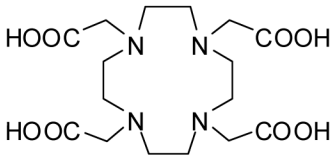

DOTA

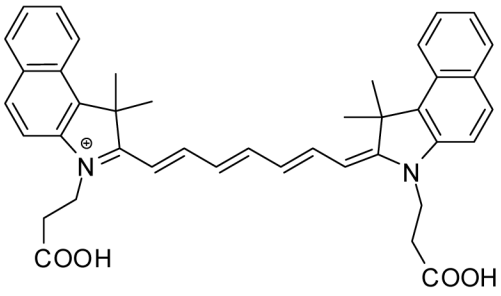

cypate

DOTA-f-cyclo-(CYwKTC)-TK (cypate)-NH_2

LS172

cypate-f-cyclo-(CYwKTC)-T -OH

cytate

Figure 1.
Structures of compounds used for this study. Lower case letters denote non-natural “D” configuration of the amino acid. DOTA and cypate are conjugated to amino groups via the carboxylic acid.

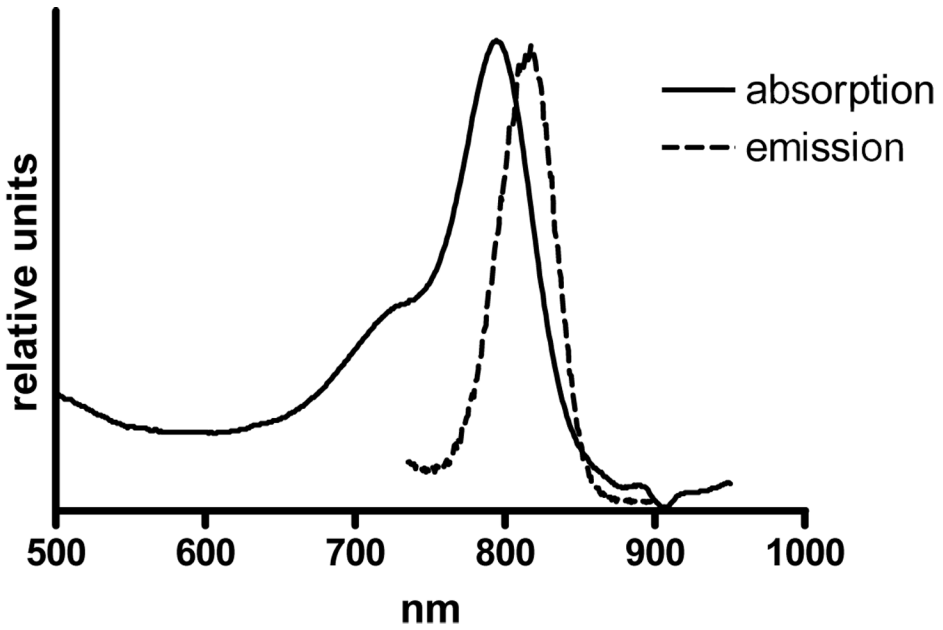

Figure 2.
Absorption and emission spectra of LS172 (100% DMSO). $\lambda_{max,abs}$ = 793 nm, $\lambda_{max,em}$ = 816 nm, Φ_F = 0.12.

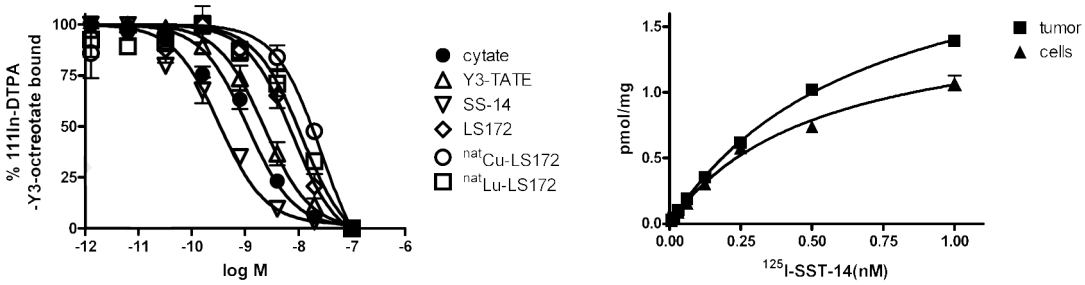

Figure 3.

A. Heterologous competitive inhibition assays with ^{111}In-DTPA-Y3-TATE on A427-7 cell membranes B. Saturation binding assays of 125I-SS-14 on membranes from A427-7 cells harvested from xenografts (tumor) or from cultured cells (cells)

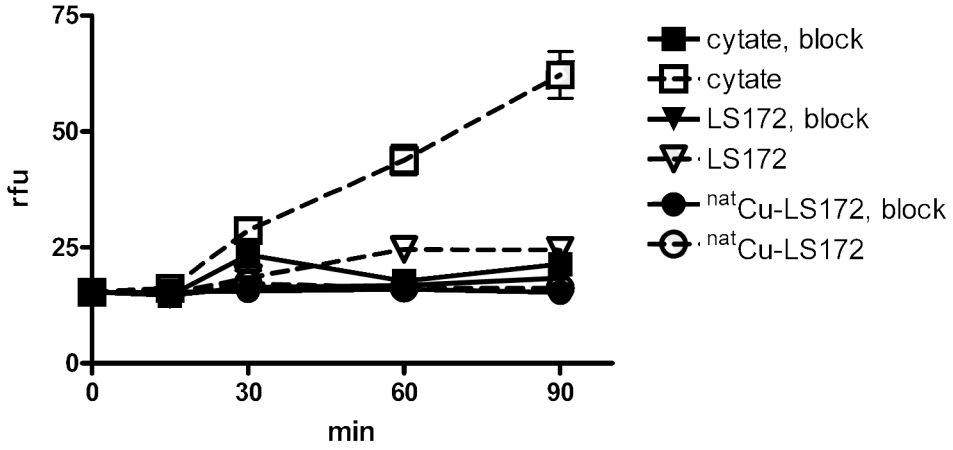

Figure 4.
Uptake of cypate-conjugated Y3-TATE analogs determined by confocal fluorescence microscopy. Cypate-conjugated Y3-TATE analogs (25nM) incubated (37°C) with A427-7 cells with and without a competitive concentration of Y3-TATE (5 μM).

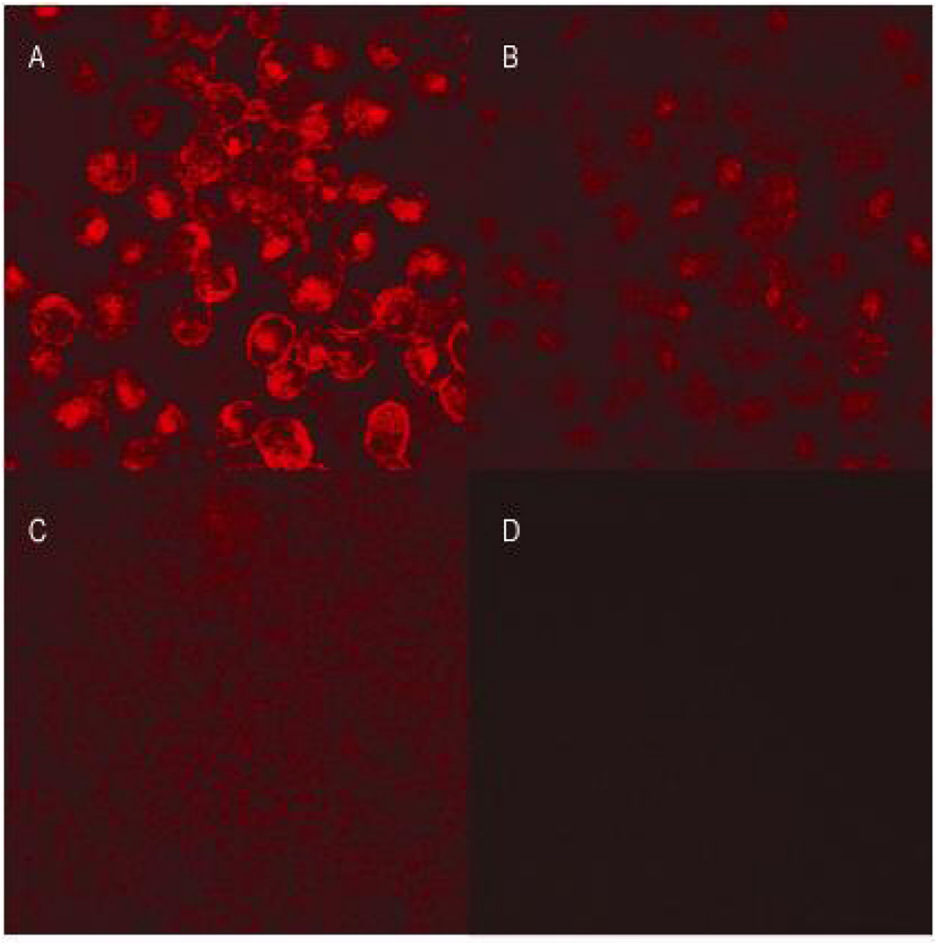

Figure 5.
Cellular uptake of NIR dye-labeled peptides in either SSTr2-positive A427-7 cells (A and B) or SSTr2-negative HEK cells (C and D) incubated with 50 nM cytate (A and C) or LS172 (B and D) for 90 min. All of the images were normalized to the highest fluorescent intensity from the image in panel A.

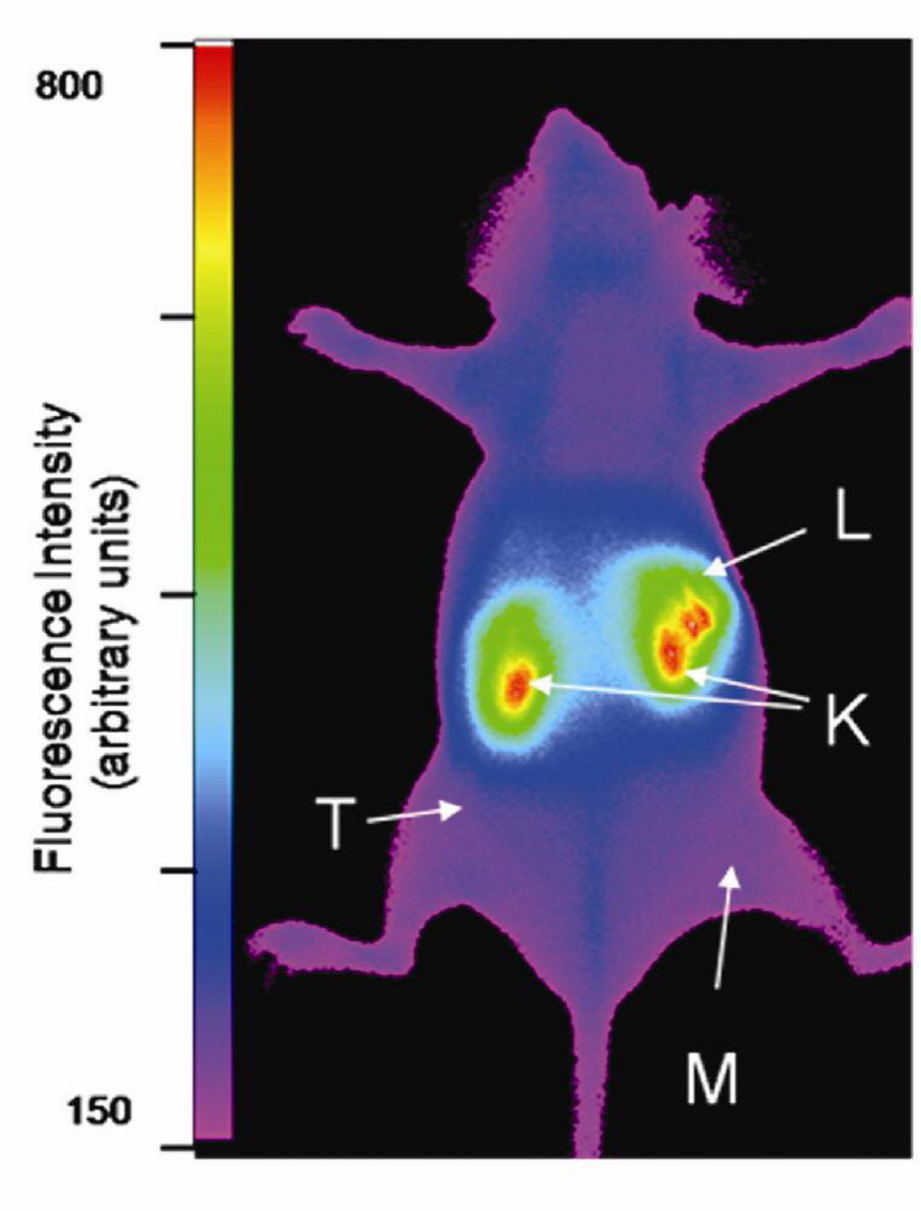

Figure 6.

Optical Biodistribution of LS172 in nude mice xenografted with A427-7 cells (24h). Representative fluorescence intensity image of a living mouse bearing a subcutaneous A427-7 xenograft 24 hs after injection of LS172. Liver (L), kidney (K), muscle (M) and tumor (T) regions of interest are indicated by arrows. The tumor is indistinguishable from surrounding muscle tissue by fluorescence intensity. Illumination light was selected with optical bandpass filter centered at 755 nm and emission captured with cooled CCD camera after 830 nm longpass filter.

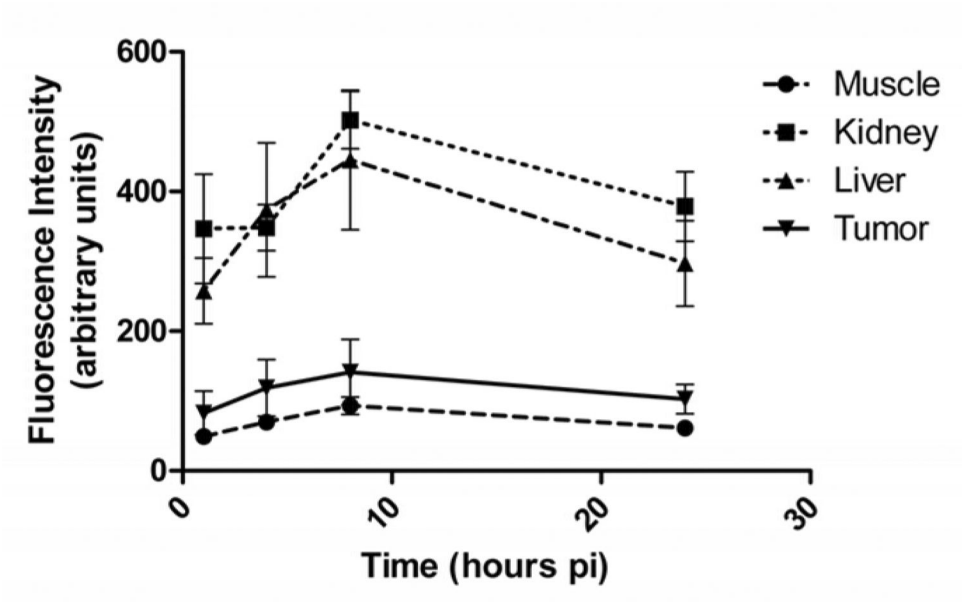

Figure 7.

Measured fluorescence intensity of selected regions of interest that indicate the accumulation of LS172 in normal muscle, kidney, liver and tumor tissues at specified time after injection of contrast agent (n=3). Fluorescence detected in the regions of the liver and kidney were significantly higher than muscle or tumor intensity for all time points. Accumulation of contrast agent in tumor tissue paralleled that of normal tissues as determined by NIR fluorescence imaging in living mice. Error bars represent SEM.

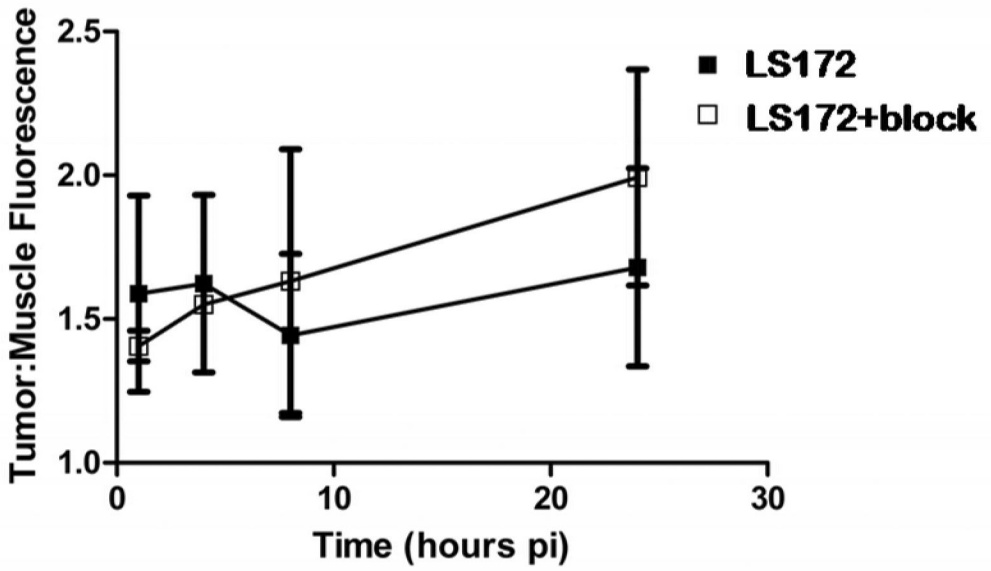

Figure 8.

Ratios of tumor to muscle fluorescence intensities measured in living mice at given timepoints after injection of LS172 (n=3) or LS172 with Y3-TATE as blocking agent (n=2). Linear regression of each data set showed the slopes were not significantly non-zero, indicating the tumor accumulation of LS172 was not different than that of normal muscle tissue. Error bars represent SEM.

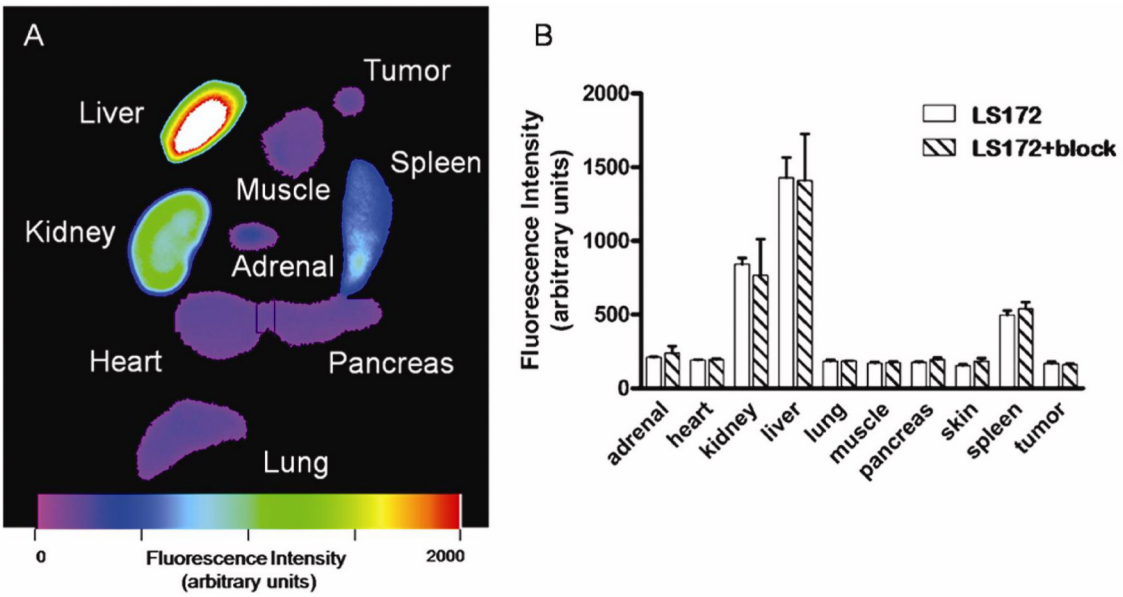

Figure 9.

A. Fluorescence intensity image of ex vivo organ tissues 24 hs after injection of LS172 representative of molecular probe biodistribution in mice. Liver, kidney and spleen tissues showed high fluorescence intensity relative to other organs. **B.** Optical Biodistribution of LS172 in nude mice xenografted with A427-7 cells (24 h).

Table 1

Heterologous competitive binding of ^{111}In-DTPA-Y3-TATE to A427-7 cell membranes (n=3 for each data point). K_i values calculated from the Cheng-Prussof equation.

competitor	IC_{50} (nM)	95% CI (nM)	K_i (nM)	95% CI (nM)
cytate	1.32	0.953 to 1.83	0.234	0.169 to 0.324
Y3-TATE	2.42	1.80 to 3.25	0.427	0.318 to 0.575
SS-14	0.375	0.265 to 0.531	0. 0660	0.0469 to 0.0939
LS172	8.13	5.62 to 11.7	2.03	1.14 to 2.94
^{nat}Cu-LS172	45.9	33.7 to 62.4	11.5	8.40 to 15.6
^{nat}Lu-LS172	8.60	4.36 to 17.0	2.15	1.09 to 4.24

Table 2

Biodistribution of ^{64}Cu-LS172 and ^{177}Lu-LS172 in AR42J tumor bearing rats at 1 h, with and without co-administration of a competing dose of Y3-TATE[a]

tissue	^{64}Cu, 1h	^{64}Cu, 1h block	^{177}Lu, 1h	^{177}Lu, 1h block
blood	0.151 ± 0.027	0.146 ± 0.019	0.228 ± 0.047	0.2250.034
lung	1.428 ± 0.738	1.081 ± 0.311	2.249 ± 0.348	1.549 ± 0.342
liver	16.824 ± 1.520	14.547 ± 5.227	17.862 ± 3.286	15.478 ± 2.829
spleen	8.069 ± 1.808	8.013 ± 2.997	5.371 ± 1.516	6.413 ± 1.734
kidney	1.138 ± 0.352	1.256 ± 0.101	1.626 ± 0.184	1.600 ± 0.202
pituitary	0.483 ± 0.538	0.085 ± 0.720	0.747 ± 0.144[b]	0.417 ± 0.232
bone	nd[c]	nd[c]	0.225 ± 0.086	0.138 ± 0.016
adrenals	0.258 ± 0.087	0.156 ± 0.060	1.037 ± 0.128[b]	0.337 ± 0.041
pancreas	0.148 ± 0.027	0.114 ± 0.022	0.307 ± 0.054[b]	0.138 ± 0.015
tumor	0.287 ± 0.046[b]	0.220 ± 0.042	0.319 ± 0.049[b]	0.139 ± 0.025

[a] Data are presented as %ID/g ± standard deviation

[b] $P < 0.05$ vs. blocked (two-tailed un-paired t-test)

[c] not determined